

Applications of the Random Coupling Model to Assess Induced Currents or Voltages in Reverberant Environment

Valentin Houchouas^{1, 2, 3, *}, Muriel Darces^{2, 3}, Marc Hélier^{2, 3},
Emmanuel Cottais¹, and José Lopes Esteves¹

Abstract—Coupling in electronic devices may be a threat for the security of the information they process. Indeed, a current flowing into a conductor may radiate an electromagnetic field that will couple onto other conductors creating parasitic signals. If this current conveys sensitive information, its confidentiality may not be guaranteed. Moreover, depending on the amplitude of these parasitic signals, dysfunction may occur. It is thus valuable to assess the coupling effects in order to evaluate the probability that a current or a voltage reaches a given magnitude. This relevant quantity may be an input for a risk analysis process.

In this study, we will focus on the study of couplings in reverberant cavities, and especially into the chassis of desktop computers. We will highlight that the Random Coupling Model (RCM) may be applied to determine statistical quantities related to induced currents or voltages between several ports placed inside a reverberant environment. Comparisons with experimental data, for several system configurations, show that the application of this model is relevant and allows to rapidly obtain the percentiles of the induced currents. At first, the coupling between two monopoles is studied, and then the coupling between printed circuit boards that are stacked together is investigated. Finally, the effect of adding broadband absorbers in casings is assessed.

1. INTRODUCTION

ElectroMagnetic SECurity (EMSEC) may be considered as the assembly of the Electromagnetic Compatibility (EMC) to the information systems security (INFOSEC). The EMSEC study of an electronic item leads to consider couplings between systems or between the elements of a system [3, 4, 13]. Indeed, if a signal carrying sensitive information couples with another system, the risk that the information is not anymore under control exists (loss of the confidentiality of information). This risk defines the TEMPEST threat. Another risk would consist of an attacker handling a malicious equipment in order to interfere with its victim's equipment nominal operation, leading to information availability or integrity losses. This type of aggression is called Intentional ElectroMagnetic Interference (IEMI).

The analysis of the electromagnetic emanations from electronic devices to recover information was firstly outlined in [28], and from then on numerous talks and papers have highlighted that threat. In [15, 22] the electromagnetic emanations from computer screens, cables, and connectors of digital video signal are processed to recover the displayed information. In [29] keyboards signals are analyzed and the keystroke information is recovered. Researches on the effects of IEMI were also conducted like in [1, 21, 23] where desktop computers are stressed by High Power ElectroMagnetic waves (HPEM).

Received 27 February 2020, Accepted 26 April 2020, Scheduled 21 May 2020

* Corresponding author: Valentin Houchouas (valentin.houchouas@ssi.gouv.fr).

¹ National Cybersecurity Agency of France, 51 Boulevard de la Tour-Maubourg, 75700 Paris 07 SP, France. ² Sorbonne Université, CNRS, Laboratoire de Génie Electrique et Electronique de Paris, Paris 75252, France. ³ Université Paris-Saclay, CentraleSupélec, CNRS, Laboratoire de Génie Electrique et Electronique de Paris, Gif-sur-Yvette 91192, France.

It is common to embed electronic devices into casings as they limit the susceptibility to the environment and their emissivity towards the environment. The casing creates reverberating conditions for the electromagnetic field. However, to the knowledge of the authors, no study has yet investigated the issue of reverberant environments from an information security viewpoint. This work is a first attempt to analyze such environments and to put forward a methodology that can be used for a risk assessment process from the EMSEC point of view. Furthermore, the great disparity and the lack of knowledge about the content (printed circuit boards, cables, fans, etc.) of equipment make deterministic approaches, like circuit models or fullwave electromagnetic simulations, non-relevant. It thus seems appropriate to favour the use of probabilistic approaches in order to characterize these phenomena by assessing occurrence probabilities of quantities of interest, such as induced currents or voltages.

Since the fifties, the application of the random matrix theory to physics problems has become more and more frequent. This method was first applied to quantum physics [7]. From then, this theory was used to solve semi-classical physics problems especially in electromagnetism where it led to the foundation of the Random Coupling Model (RCM) [32, 33]. This method seems to be well suited for the above-mentioned problem, and will be explored in the rest of the paper.

At first, the RCM will be described. Its assumptions and conditions of application will be reminded. Then, some guidelines will be provided in order to efficiently implement that method. Finally, the RCM will be applied to two different configurations: the coupling between monopoles and the coupling between microstrip transmission lines. Experimental data will be compared to RCM based simulations. An experimental setup that allows to create a reverberant environment will be detailed. In addition, and for the last configuration, the effect of placing absorbers in the reverberant environment will be assessed through statistical quantities.

2. THE RANDOM COUPLING MODEL

2.1. Description

The Random Coupling Model is a statistical circuit model where the links between the ports of a reverberant system are represented by a cavity impedance matrix $\underline{\underline{Z}}^{\text{cav}}$. A port may be the end of a cable, of a transmission line or the input of an antenna for example. The eigenmodes density needs to be high enough in the system so that the cavity can be considered as a chaotic one [33]. This is a mandatory requirement to apply the RCM. A criterion will be given below to evaluate the chaoticity of a system [5, 17]. Two behaviors are merged into the RCM. The first one is related to the coupling between ports that would happen in free space, i.e., without boundary conditions that make the system reverberant. For an electronic equipment, this can be done by removing its casing or by placing absorbers against the casing wall [19]. This behavior is characterized by a radiation impedance matrix $\underline{\underline{Z}}^{\text{rad}}$ which is frequency-dependent. This impedance may be determined either by simulations, by measurements in an anechoic chamber or by an ad hoc model. The second behavior takes into account the reverberating effects of the cavity due to the casing. The normalized impedance matrix $\underline{\underline{\xi}}$, that depends on the boundary conditions of the system, models the couplings between the ports and the eigenmodes of the cavity. From $\underline{\underline{Z}}^{\text{rad}}$ and $\underline{\underline{\xi}}$, the cavity impedance $\underline{\underline{Z}}^{\text{cav}}$ is defined as [33]:

$$\underline{\underline{Z}}^{\text{cav}} = j\Im \left\{ \underline{\underline{Z}}^{\text{rad}} \right\} + \left[\Re \left\{ \underline{\underline{Z}}^{\text{rad}} \right\} \right]^{1/2} \underline{\underline{\xi}} \left[\Re \left\{ \underline{\underline{Z}}^{\text{rad}} \right\} \right]^{1/2} \quad (1)$$

symbols $\Re[\cdot]$ and $\Im[\cdot]$ denote respectively the real and imaginary parts of a complex quantity. The normalized random matrix $\underline{\underline{\xi}}$ may be expressed as:

$$\underline{\underline{\xi}}(k) = -\frac{j}{\pi} \sum_{n=1}^M \frac{\Delta k^2 \vec{\Phi}_n \otimes \vec{\Phi}_n^T}{k^2(1 - j/Q) + k_n^2} \quad (2)$$

The random vector $\vec{\Phi}_n$, whose components are distributed according to a normal distribution with zero mean and unit standard deviation $\mathcal{N}(0, 1)$, is responsible for the couplings between the M modes of the cavity and its N ports (\otimes refers to the outer product). The summation over n accounts for the M

modes (associated to the wavenumbers k_n) taken into account inside the cavity. k is the wavenumber of interest and Δk^2 the so-called mean spacing between two adjacent wavenumbers ($\Delta k^2 = \langle k_{n+1}^2 - k_n^2 \rangle$). Q is the quality factor of the unloaded cavity (without the ports) [19].

In a statistical approach, the interest is not focused on a specific cavity but on a set of various ones. Instead of determining the modes of the cavity, these are randomly drawn in accordance with the random matrix theory [19]. Indeed, WIGNER finds that the statistics of the eigenlevel spacings of the Hamiltonian of some systems are the same as those of the eigenvalues of random matrices of a given ensemble [7]. Moreover, the BERRY hypothesis states that, for a chaotic cavity, an infinite sum of isotropic plane waves is a good statistical model to describe the eigenfunctions [2, 12]. The RCM combines both conceptual features.

Equation (2) may be rewritten as [19]:

$$\underline{\underline{\xi}} = -\frac{j}{\pi} \underline{\underline{W}} [\underline{\underline{\lambda}} - j\alpha \underline{\underline{1}}]^{-1} \underline{\underline{W}}^T \quad (3)$$

where $\underline{\underline{W}}$ is a $M \times N$ real matrix, N the number of ports in the system, and M the number of modes taken into account into the cavity. The elements of $\underline{\underline{W}}$ are normally distributed ($W_{ij} \sim \mathcal{N}(0, 1)$). $\underline{\underline{W}}$ represents the coupling of the modes to the ports of the system. $\underline{\underline{\lambda}}$ is a diagonal matrix populated with the eigenvalues of a matrix from the Gaussian Orthogonal Ensemble (GOE). From the random matrix theory, we know that the spacing between these sorted eigenvalues has the same statistical distribution than Δk^2 [24]. The GOE ensemble is chosen since the system is time-reversal invariant [19]. The loss parameter α may be processed from the quality factor Q of the cavity, as $\alpha = \frac{k^2}{Q\Delta k^2}$.

In this paper, the question of short orbits [14, 31] is not handled. Short orbits are ray trajectories that do not ergodically travel inside the cavity. Instead, the ray leaves a port and directly returns to another one [12]. Another formulation of the RCM should be used to take them into account.

To determine the statistics of $\underline{\underline{Z}}^{\text{cav}}$, a large number of MONTE-CARLO iterations are performed. For each iteration, a matrix $\underline{\underline{\xi}}$ is randomly drawn (as $\underline{\underline{Z}}^{\text{rad}}$ is deterministic). These iterations are time-consuming, therefore some optimizations may be implemented.

2.2. Implementation of the RCM

To obtain reliable probability density functions (e.g., in order to compute probabilities of rare events), numerous draws must be carried out. With a naive implementation of Equation (3), thousands of draws are calculated within a few hours. To reduce computation time, several optimizations may be realized. First, the use of a compiled language rather than an interpreted one (like Python or MATLAB) increases the performances. Moreover, calling libraries dedicated to efficient matrix computations results in a performance gain. It was chosen to take advantage of the *Math Kernel Library* (MKL) from INTEL. We can explain how the MKL is used for three steps that occur while programming the RCM:

- Eigenvalues of a real symmetric matrix $\underline{\underline{A}}$: the function `dsyevd` is used, which implements the divide and conquer algorithm. This algorithm is dedicated to real symmetric matrices;
- Square root of a real symmetric matrix $[\underline{\underline{A}}]^{1/2}$: by using the `dsyevd` function, the matrix $\underline{\underline{A}}$ is diagonalized ($\underline{\underline{A}} = \underline{\underline{B}} \underline{\underline{\lambda}} \underline{\underline{B}}^{-1}$). Then, the square root of each element of $\underline{\underline{\lambda}}$ is extracted, obtaining $\underline{\underline{\lambda}}^{1/2}$. Then, we compute $\underline{\underline{B}} \underline{\underline{\lambda}}^{1/2} \underline{\underline{B}}^{-1}$ by using the function `zgemm` (product of general complex matrices);
- Inverse of a complex matrix $[\underline{\underline{A}}]^{-1}$: first the LU factorization of the matrix $\underline{\underline{A}} = \underline{\underline{L}} \underline{\underline{U}}$ is performed thanks to `zgetrf`. Then, the backward and forward substitutions are computed by the function `zgetri`.

The dedicated codes are also designed to be multithreaded, allowing to split the computations and to process them in parallel. This requires to design the programs in such a way that resources are well dispatched between the different threads. Fig. 1 shows the performance gains to compute 300

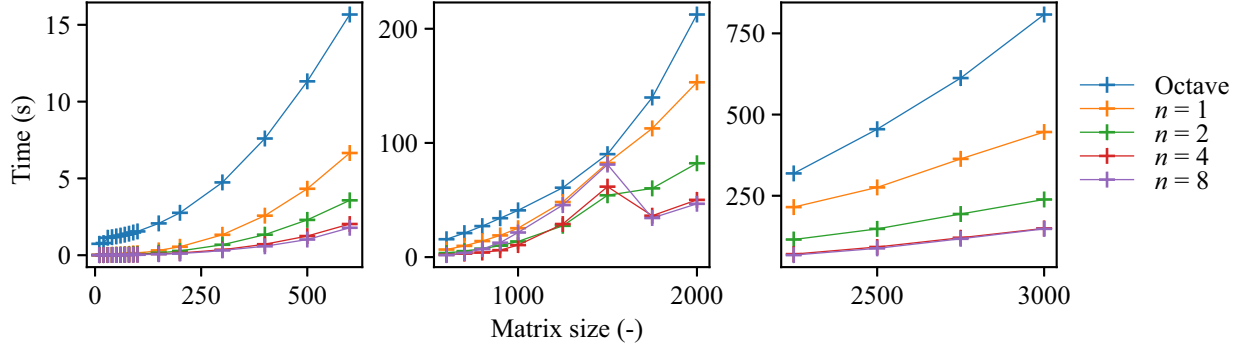


Figure 1. CPU time required to compute the eigenvalues of matrices from the GOE (based on 10 runs). Octave refers to the implementation proposed by the author of the RCM [18] and runs with Octave [6], and n is the number of threads used to compute the eigenvalues using the listed optimizations. Symbol (-) denotes a dimensionless quantity. Note that for $n > 4$ there is no performance gain as the computer has only 4 physical cores.

matrices $\underline{\underline{\lambda}}$ versus different matrix sizes M . However, it is important to avoid using the simultaneous multithreading technique (virtual cores) to be able to take advantage of the CPU caches. Some matrices have large dimensions leading to high computation cost when it comes to multiply matrices. By noticing that matrix $[\underline{\underline{\lambda}} - j\alpha\underline{\underline{1}}]^{-1}$ is diagonal, it is easy to reduce the computational complexity from $O(M^2N)$ to $O(MN)$ when making the product $\underline{\underline{W}}$ by $[\underline{\underline{\lambda}} - j\alpha\underline{\underline{1}}]^{-1}$. By combining all these optimizations, it is possible to obtain induced currents and voltages within less than 4 minutes for thousands of draws of the matrix $\underline{\underline{Z}}^{\text{cav}}$. These results have been obtained on an Intel(R) Core(TM) i7-4770 CPU (3.40 GHz) with 32 GB of random access memory and a SSD hard drive.

To deploy the RCM, some results do not need to be computed at each run, like the set of matrices $\underline{\underline{\lambda}}$. $\underline{\underline{\lambda}}$ is a diagonal matrix whose elements are the eigenvalues of a random matrix from the GOE ensemble. As this matrix is not attached to a specific application, it is possible to precompute numerous matrices $\underline{\underline{\lambda}}$.

Three independent codes have been implemented to apply the RCM: one to precompute a set of matrices $\underline{\underline{\lambda}}$, a second one to implement Equation (1), and a last one to compute $\underline{\underline{\xi}}$ from Equation (3). The latter is in charge of computing many matrices $\underline{\underline{\xi}}_\alpha$ for different values of the loss parameter α . From $\underline{\underline{\xi}}_\alpha$, the probability density functions of the elements $\xi_{ij\alpha}$ are determined by applying a kernel density estimation [30] and then are stored. These statistical distributions will be used to fit the elements $\xi_{ij}^{\text{Measurements}}$ obtained experimentally in order to determine the loss parameter α_{fit} .

3. COMPARISON WITH EXPERIMENTAL DATA

3.1. Measurement Setup

To compare the RCM results with experimental ones, a mock-up of a computer chassis (Fig. 2) has been designed. Exchangeable front and back panels were chosen to be able to use the same mock-up for several configurations. This mock-up is 400 mm high, 440 mm deep and 170 mm wide. The panels are screwed to the mock-up body and, for reproducibility purpose, the screws are tightened with a torque screwdriver. The design of this mock-up and the validation of its performances have already been assessed [20]. In order to obtain statistics on the magnitude of induced currents or voltages for a large number of casing geometries, i.e., for different boundary conditions, a small mode stirrer has been fabricated and installed inside the mock-up (see Fig. 10(c)). It is composed of two blades attached to a dielectric rod mechanically coupled with the drive shaft of a stepper motor. The motor is set outside the mock-up (Fig. 10(b)). For each stirrer angle, a measurement of the scattering matrix $\underline{\underline{S}}$ is performed thanks to a Vector Network Analyzer (VNA). 360 stirrer angles will be considered to

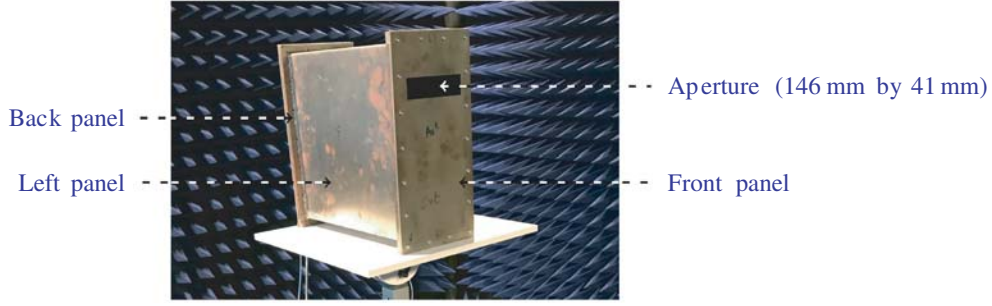


Figure 2. Picture of the mock-up.

generate the results. In the following sections, that mock-up associated to the stirrer will be used to measure the couplings between monopoles at first, and then between stacked printed circuit boards. This experimental results will be compared to those produced by the RCM.

The experimental impedance matrix is computed from the scattering matrix $\underline{\underline{S}}$ as:

$$\underline{\underline{Z}}^{\text{Measurements}} = [Z_0 \underline{\underline{1}}]^{\frac{1}{2}} (\underline{\underline{1}} + \underline{\underline{S}}) (\underline{\underline{1}} - \underline{\underline{S}})^{-1} [Z_0 \underline{\underline{1}}]^{\frac{1}{2}} \quad (4)$$

where $\underline{\underline{1}}$ is the identity matrix, and Z_0 is the characteristic impedance of the VNA ports, i.e., $Z_0 = 50 \Omega$. Then the induced currents are computed in the same way as for the measured and simulated (RCM) data from:

$$\vec{I}^{\text{Measurements/RCM}} = (\underline{\underline{Z}}^{\text{Measurements/cav}} + Z_0 \underline{\underline{1}})^{-1} \begin{bmatrix} \sqrt{2Z_0 P_1} \\ \vdots \\ \sqrt{2Z_0 P_N} \end{bmatrix} \quad (5)$$

where P_i is the power injected into the port i of the system. As a VNA is used, the excitation source is a frequency sweep.

3.2. Methods to Determine the Parameters of the Random Coupling Model

Three quantities need to be determined to apply the RCM: the free space impedance matrix $\underline{\underline{Z}}^{\text{rad}}$, the number of modes M taken into account inside the cavity and the loss parameter α . The free space impedance matrix $\underline{\underline{Z}}^{\text{rad}}$ for all the tested configurations has been determined from experimental data acquired by a VNA in free space (see Fig. 5 for the monopoles and Fig. 10(a) for a stacking of printed circuit boards). Setting M is a trade-off between the number of modes to consider inside the cavity and the computation time. As the RCM applies only for chaotic cavities (thus overmoded), M must not be small. In the literature, two values are commonly found: $M = 600$ in [10, 11], and $M = 200$ in [32]. The impact on the PDF of the elements of $\underline{\underline{\xi}}$ as M increases is given in Fig. 3. It can be shown that the real part of the elements ξ_{11} converges rapidly as M increases. The other elements ξ_{ij} for both the real and imaginary parts follow the same behavior. Thus, in what follows, M is set to 600 as a trade-off.

The parameter α is the more difficult one to assess. It characterizes the losses inside the cavity and is frequency-dependent. Several techniques may be applied to evaluate it, as explained in [9, 19], based on experimental data. The first method is to compute and to store the PDF of the elements of $\underline{\underline{\xi}}_\alpha$ for different values of α . Then, from acquired data, $\underline{\underline{\xi}}^{\text{Measurements}}$ is computed by inverting (1) as:

$$\underline{\underline{\xi}}^{\text{Measurements}} = \Re \left[\underline{\underline{Z}}^{\text{rad}} \right]^{\frac{1}{2}} \left(\underline{\underline{Z}}^{\text{cav}} - \Im \left[\underline{\underline{Z}}^{\text{rad}} \right] \right) \Re \left[\underline{\underline{Z}}^{\text{rad}} \right]^{\frac{1}{2}} \quad (6)$$

A fitting process then allows to match the elements of $\underline{\underline{\xi}}^{\text{Measurements}}$ with the elements of the matrices $\underline{\underline{\xi}}_{\alpha=\alpha_{\min}}, \dots, \underline{\underline{\xi}}_{\alpha=\alpha_{\max}}$. The best fit determines the value of α .

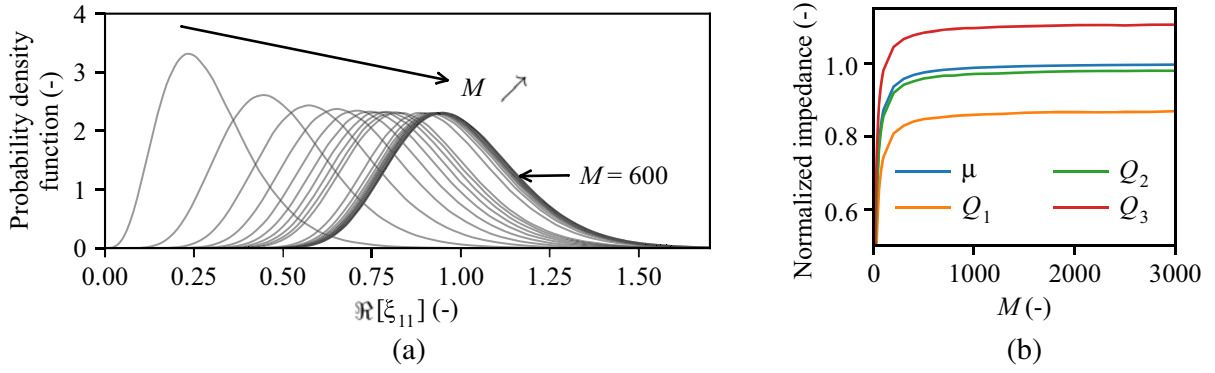


Figure 3. Variations of the PDF of the real part of the elements ξ_{11} for a loss parameter $\alpha = 10$ and for a two-ports system versus M . (a) PDF of the real part of the element ξ_{11} for M between 10 and 3000. The PDF converges rapidly as M increases. (b) Mean μ , first Q_1 , second (median) Q_2 and third Q_3 quartiles of the elements $\Re[\xi_{11}]$ according to M .

The second method computes α from [9]:

$$\text{Var} [\Re [\xi_{ii}^{\text{Measurements}}]] = \text{Var} [\Im [\xi_{ii}^{\text{Measurements}}]] = \frac{1}{\pi\alpha_{ii}} \quad (7)$$

$$\text{Var} [\Re [\xi_{ij}^{\text{Measurements}}]] = \text{Var} [\Im [\xi_{ij}^{\text{Measurements}}]] = \frac{1}{2\pi\alpha_{ij}} \quad (8)$$

then $\alpha = \frac{1}{N^2} \sum_{i,j} \alpha_{ij}$ (where $\text{Var} [\cdot]$ stands for the variance). The benefit of this latter method is that no $\underline{\xi}_{\alpha}$ matrix needs to be computed. However, it is important to note that for both methods, the determination of α relies on experimental data. Both methods have been employed in this work. A comparison can be found between them in [9].

3.3. Coupling between Two Monopoles

The first application of the RCM is about the coupling between two monopoles that are placed inside a cavity. The scattering matrix \underline{S} between the two monopoles placed in a computer chassis mock-up is measured between 10 and 26.5 GHz, and for 360 stirrer angular positions. Then the free space impedance $\underline{Z}^{\text{rad}}$ is measured (see Fig. 5). Both monopoles are composed of a 46 mm long wire soldered to a bulkhead through hole SMA connector (see Fig. 4). The aim is to determine the Probability



Figure 4. A monopole attached to the front panel.

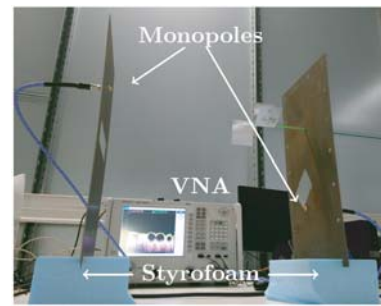


Figure 5. Setup to measure the free space impedance $\underline{Z}^{\text{rad}}$ between two monopoles (front panel on the left, back panel on the right). Two blocks of styrofoam are used as stands.

Density Functions (PDF) of the voltage induced on the port of one monopole when the other one is transmitting. This configuration is similar to the one presented in [9] or in [16]. However, in [9], the free-space impedance was approximated as $\underline{\underline{Z}}^{\text{rad}} = [Z_0 \underline{\underline{1}}]^{\frac{1}{2}} (\underline{\underline{1}} + \langle \underline{\underline{S}} \rangle) (\underline{\underline{1}} - \langle \underline{\underline{S}} \rangle)^{-1} [Z_0 \underline{\underline{1}}]^{\frac{1}{2}}$, where $\langle \underline{\underline{S}} \rangle$ is the mean scattering matrix over the 360 stirrer angular positions. In [16], the free-space impedance was determined by either installing absorber materials on the cavity walls to simulate a free space behavior, or by a full-wave simulation. In the present work, the free-space impedance is measured with monopoles set in genuine free-space conditions.

3.3.1. Evaluation of the System Chaoticity

As mentioned above, the RCM applies only to chaotic systems. In [5, 17] a method is proposed to determine if a system is chaotic or not, which is based on the properties of the eigenvalues of the normalized scattering matrix of the system. It specifies that the phase of the eigenvalues has to be uniformly distributed, and that the phase and magnitude of the eigenvalues need to be independent. From the normalized impedance $\underline{\underline{\xi}}^{\text{Measurements}}$, the normalized scattering matrix $\underline{\underline{s}}$ is computed and diagonalized:

$$\underline{\underline{s}} = (\underline{\underline{\xi}}^{\text{Measurements}} - \underline{\underline{1}}) (\underline{\underline{\xi}}^{\text{Measurements}} + \underline{\underline{1}})^{-1} \quad (9)$$

$$\underline{\underline{s}} = \underline{\underline{U}} \begin{pmatrix} |\lambda_1| e^{j\phi_{\lambda_1}} & \cdots & 0 \\ \vdots & \ddots & \vdots \\ 0 & \cdots & |\lambda_N| e^{j\phi_{\lambda_N}} \end{pmatrix} \underline{\underline{U}}^{-1} \quad (10)$$

where $\underline{\underline{U}}$ is the change of basis matrix.

Figure 6 depicts, for four adjacent frequency bands, histograms of the real and imaginary parts of the eigenvalues of $\underline{\underline{s}}$ and of their phases. We can state that the system, composed of the two monopoles into the mock-up fitted with the stirrer, is a chaotic system. Thus, the RCM can be applied.

3.3.2. Fitting of the Loss Parameter α and PDF of the Induced Voltages

At the center of each four frequency bandwidths for which the chaoticity of the system has been evaluated (i.e., 7.5, 12.5, 17.5 and 22.5 GHz), the loss parameter α has been determined. As previously explained, a fitting process allows to fit the PDF of the elements of $\underline{\underline{\xi}}^{\text{Measurements}}$ to that of the elements of $\underline{\underline{\xi}}_{\alpha}$. Frequency samples within a bandwidth of 500 MHz acquired for 360 stirrer positions have been gathered to compute the PDF of the elements of $\underline{\underline{\xi}}^{\text{Measurements}}$. Fig. 7 depicts the PDF of the real part of ξ_{ij} and the fitted PDF associated to a given loss parameter α . We notice that α increases as the frequency does. This phenomenon complies with the results given in [9].

We highlight the fact that fitting only the off-diagonal elements (ξ_{12} and ξ_{21}) gives results closer to experimental data when it comes to compute the induced voltages. Fig. 8 shows the comparison between the PDF of the induced voltages computed from experimental data and the PDF obtained from RCM simulations. A good agreement can be noticed for all four frequencies. Moreover, we observe that the induced voltages decrease when the frequency rises.

3.4. Application of the RCM to the Coupling between Stacked Printed Circuit Boards within Computer Chassis

In this section, we will assess the probabilities of occurrence of induced currents at one end of microstrip transmission lines. These transmission lines are printed on circuit boards that are stacked together and placed into a cavity with changing boundary conditions (by using the stirrer). These configurations can be representative of a computer chassis in which cables are not constrained (in such a way that they can move), or when an unwanted mechanical constraint of the chassis occurs and change the boundary conditions of the problem. This may also obviously happen when additional parts are integrated inside

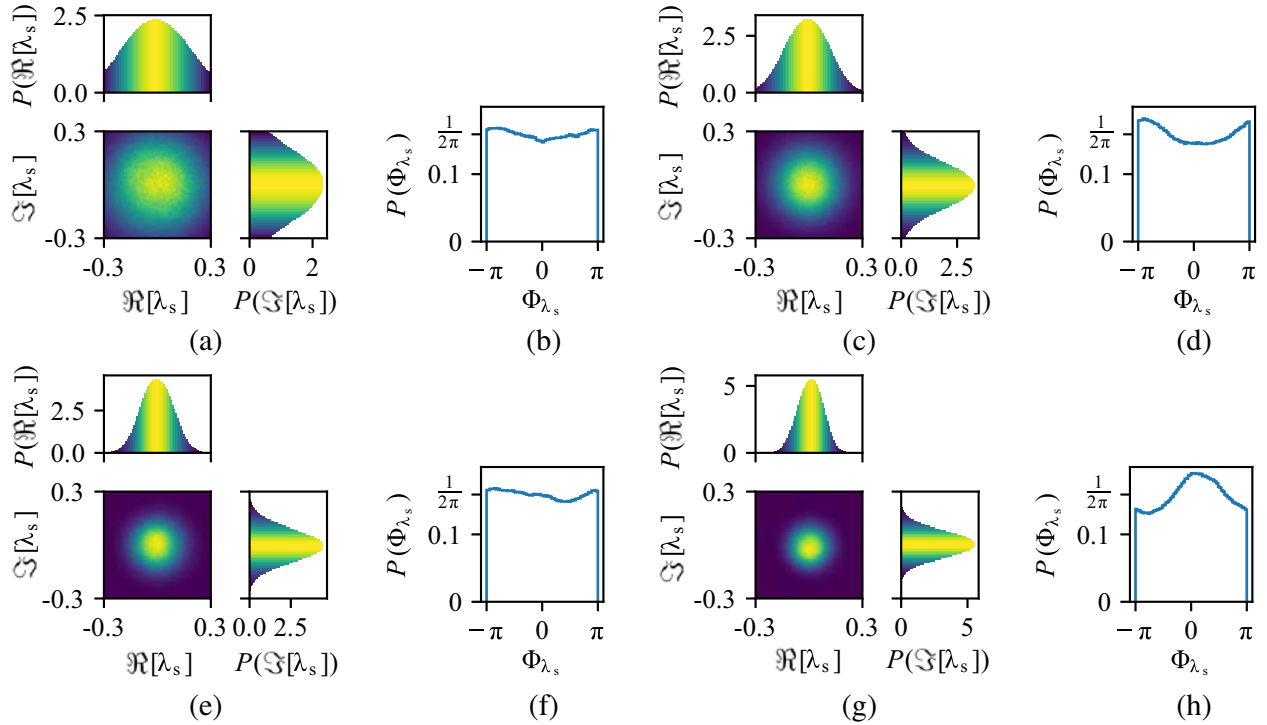


Figure 6. (a), (c), (e), and (g) show the 2D histograms of the real $\Re[\lambda_s]$ and imaginary $\Im[\lambda_s]$ parts of the eigenvalues of the matrix $\underline{\underline{s}}$, and (b), (d), (f), and (h) present the distribution $P(\Phi_{\lambda_s})$ of the phase of the eigenvalues of $\underline{\underline{s}}$. As the 2D histogram is rotation invariant and as $P(\Phi_{\lambda_s})$ is almost uniformly distributed $P(\Phi_{\lambda_s}) \approx \mathbb{1}_{[-\pi, \pi]}(\Phi_{\lambda_s}) \frac{1}{2\pi}$ we consider that the system is chaotic. (a) 5 to 10 GHz. (b) 5 to 10 GHz. (c) 10 to 15 GHz. (d) 10 to 15 GHz. (e) 15 to 20 GHz. (f) 15 to 20 GHz. (g) 20 to 25 GHz. (h) 20 to 25 GHz.

the chassis. The final objective is to be able to provide placement rules of the boards inside the chassis, and to minimize, if possible, the probability that a current magnitude exceeds a given threshold.

To the knowledge of the authors, this work is the first comparison between measurements and RCM simulations for systems with more than two ports. Moreover, as already mentioned, in previous works related to the RCM, only monopoles were considered, as in [9, 16]. We focus here on configurations with more complex ports, i.e., PCBs, and more complex arrangements between the ports.

3.4.1. Tested Configurations

Several stacking configurations (Table 1) composed of a maximum of four printed circuit boards (PCB) (Fig. 9) are considered. On each board a microstrip transmission line (characteristic impedance 50Ω) is printed, terminated at one end by a bulkhead through hole SMA connector (that also allows to hold the PCB in the mock-up) and at the other end by a 50Ω load (surface mount resistor and via). Each PCB can be installed at a chosen location (among four) in the stacking. Notice that some locations may be left empty. Position 1 of a board corresponds to the lower location of the stacking, and position 4 to the upper location (Fig. 10(d)). Two consecutive positions are spaced by a 2 cm gap (like in a real desktop computer). The first location is at a height of 5 cm above the bottom of the mock-up, and the left edge of the boards is next to the left panel of the mock-up (see Fig. 2 and Fig. 9(a)). These configurations were chosen to allow to test the RCM with configurations that present different spacings (multiple of 2 cm) between the boards, thus different modal configurations of the electromagnetic field within the stacking.

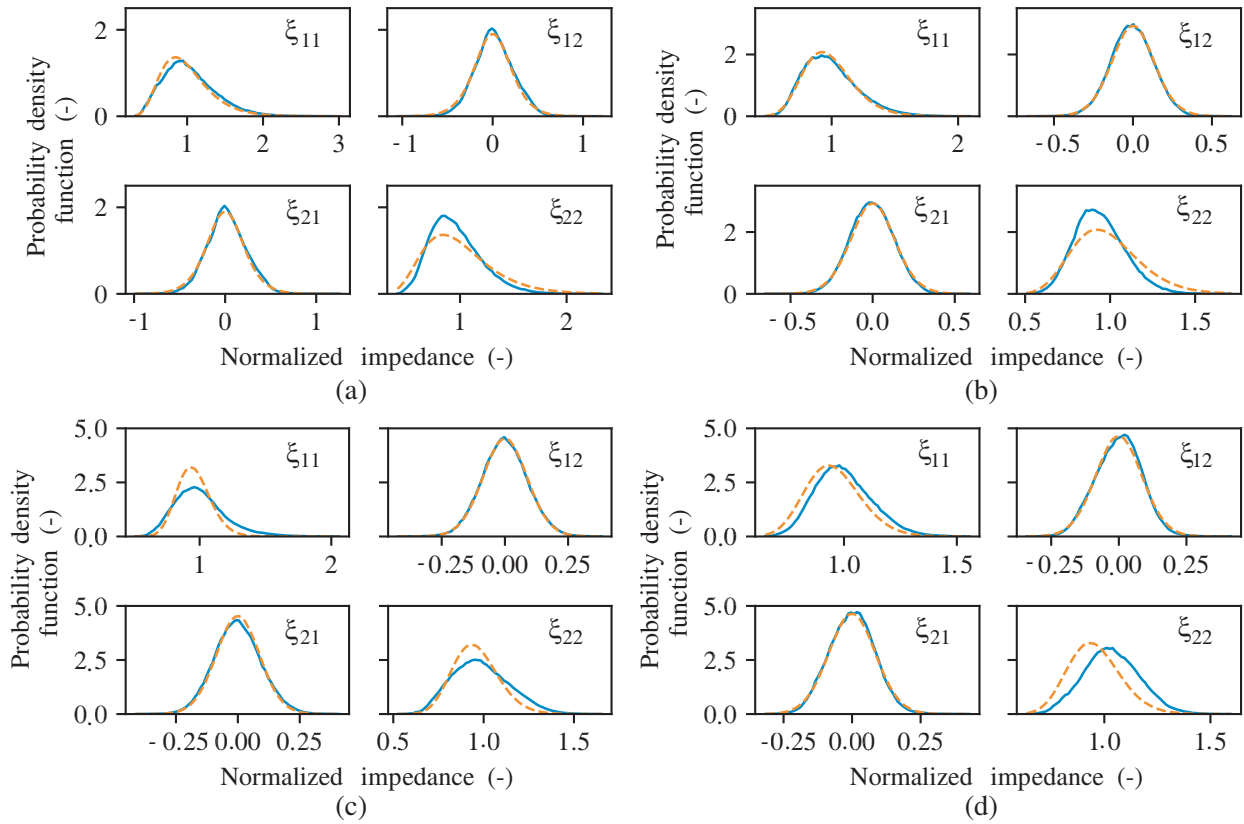


Figure 7. Probability density functions of the real part of the elements ξ_{ij} from $\underline{\xi}^{\text{Measurements}}$ (blue curves) and from $\underline{\xi}_{\alpha}$ (dashed orange curves). (a) 7.5 GHz, $\alpha_{\text{fit}} = 3.1$. (b) 12.5 GHz, $\alpha_{\text{fit}} = 8$. (c) 17.5 GHz, $\alpha_{\text{fit}} = 20$. (d) 22.5 GHz, $\alpha_{\text{fit}} = 21$.

Table 1. The five configurations considered. The number prefixed by the symbol # corresponds to the port index of the board for a given configuration. For example, configuration C4 corresponds to a stacking of two boards (“L right” and “L left”), installed at the positions 1 and 3. The board “L right” is connected to the first port of the VNA (port index #1) and the board “L left” to its second port (port index #2). As the position 2 is left empty, a 4 cm gap spaces the two boards.

Configuration	Number of ports N	Position 1	Position 2	Position 3	Position 4
C1	4	Meander #1	Straight #2	L right #3	L left #4
C2	4	L right #1	Meander #2	L left #3	Straight #4
C3	2	L right #1	-	-	L left #2
C4	2	L right #1	-	L left #2	-
C5	3	Meander #1	Straight #2	-	L left #3

3.4.2. Computing of the Experimental Results

The scattering parameters \underline{S} between the N ports of the system have been measured from 10 to 26.5 GHz with a step of 1 MHz (16501 frequency samples), and for 360 stirrer positions. Using \underline{S} and Equation (4), $\underline{Z}^{\text{Measurements}}$ is calculated, then the current vector \vec{I}^{RCM} is computed from Equation (5). Fig. 11 and Fig. 12 show the cumulative distribution functions (CDF) $|I_{\#a,Cb,\#i}^{\text{Measurements}}|$ of the measured current

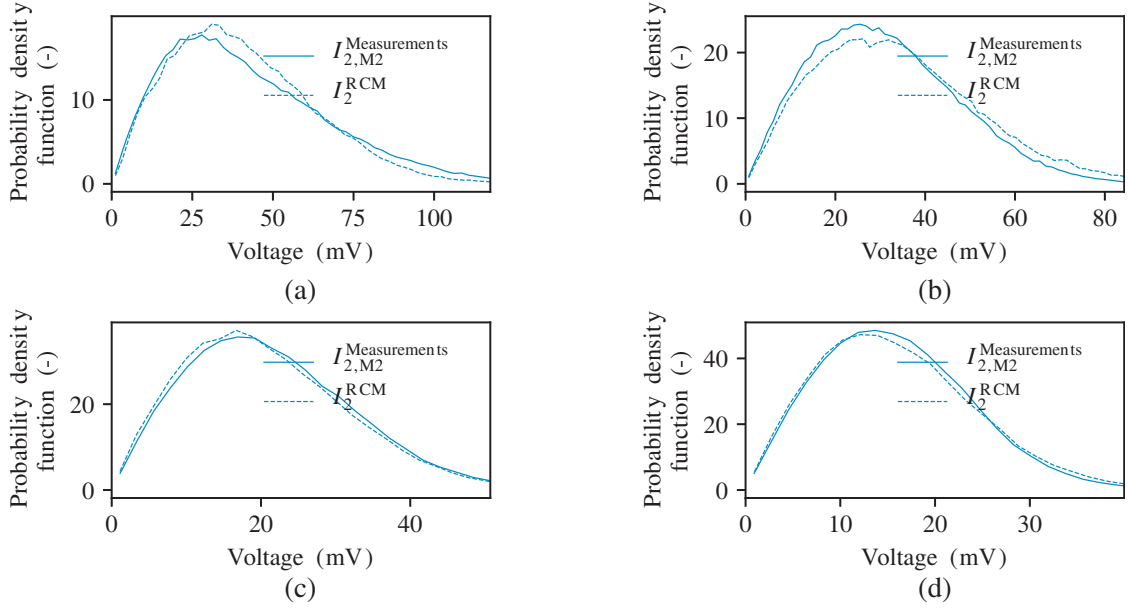


Figure 8. Comparison between the probability density functions of the magnitude of the induced voltages on port 2, measured and simulated by the RCM. These PDF are computed within a frequency bandwidth of 500 MHz, and with a loss factor α_{fit} considered as constant within the bandwidth. (a) 7.5 GHz, $\alpha_{\text{fit}} = 3.1$. (b) 12.5 GHz, $\alpha_{\text{fit}} = 8$. (c) 17.5 GHz, $\alpha_{\text{fit}} = 20$. (d) 22.5 GHz, $\alpha_{\text{fit}} = 21$.

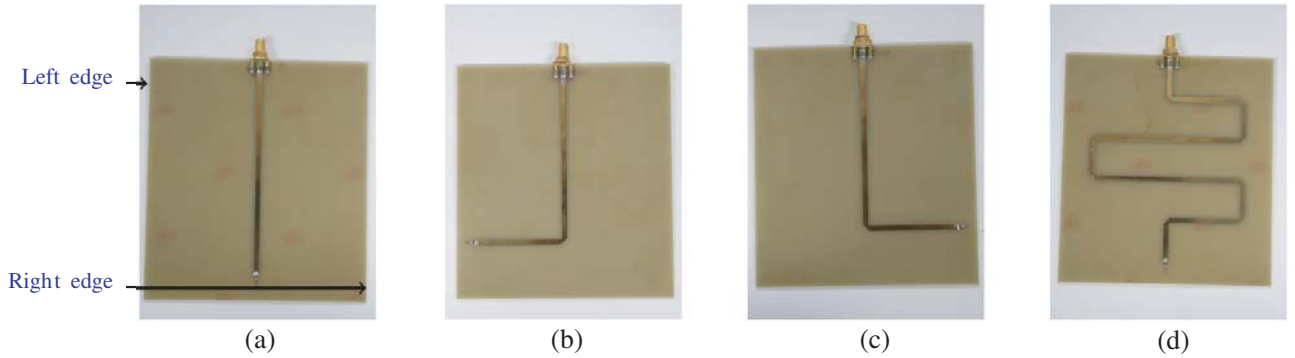


Figure 9. The four available boards used in the stacking. Each board is 12 cm wide and 13 cm long. (a) Straight. (b) L left. (c) L right. (d) Meander.

amplitudes, where:

- a corresponds to the port index number. It merges with the port index of the VNA where the transmission line is connected to;
- b is the configuration number as listed in Table 1;
- i corresponds to the source port index. Thus, only P_i is not null in Equation (5). In Fig. 11 the power is injected into port index #1 ($P_1 = 10$ dBm) and in Fig. 12 into the port index #2 ($P_2 = 10$ dBm).

3.4.3. Computing of the RCM Results

The matrices $\underline{\underline{Z}}^{\text{rad}}$ have been measured in free space (see Fig. 10(a)) for the five configurations. The loss parameter α has been determined from Equations (7) and (8) using $\underline{\underline{\xi}}^{\text{Measurements}}$ (computed from

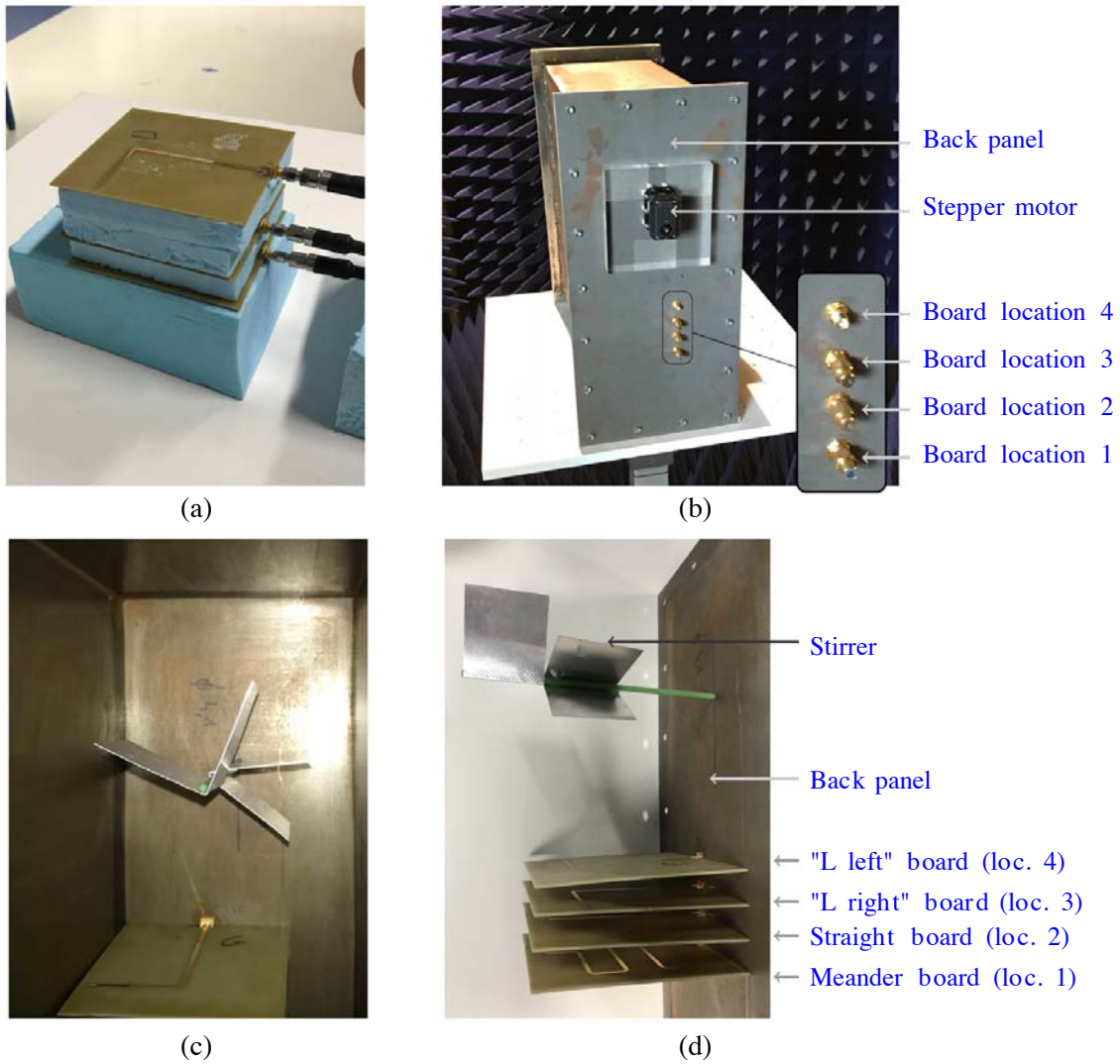


Figure 10. Illustrations of the experimental setup. (a) Example of measurement of the free space impedance $\underline{Z}^{\text{rad}}$. (b) The stepper motor and SMA connectors of four boards, attached to the back panel of the mock-up. This situation may depict either configurations $C1$ or $C2$. (c) The stirrer inside the mock-up. (d) The stacking of four printed circuit boards attached on the back panel of the mock-up. This picture shows configuration $C1$, as listed in Table 1.

$\underline{Z}^{\text{Measurements}}$ with Equation (6)), as $\alpha = \frac{1}{N^2} \sum_{i,j} \alpha_{i,j}$ with N the number of ports in the system. Then, from Equation (1), 360×16501 matrices $\underline{Z}^{\text{cav}}$ have been computed as well as the port currents vector \vec{I}^{RCM} (from Equation (5)). Depending on N , the time needed to compute the 5940360 vectors \vec{I}^{RCM} varies from 40s to 3min. Likewise, Fig. 11 and Fig. 12 display the CDF $|I_{\#a,Cb,\#i}^{\text{RCM}}|$ of the simulated current amplitudes.

3.4.4. Discussion

The results depend on the existence of a line of sight configuration between the source board and the other ones. The line of sight case appears for example when the source port index is #1 and the measurement port index is #2, or when the source port index is #2 and the measurement port indexes are #1 and #3. There is a good agreement between the CDF of the simulated data and the measured

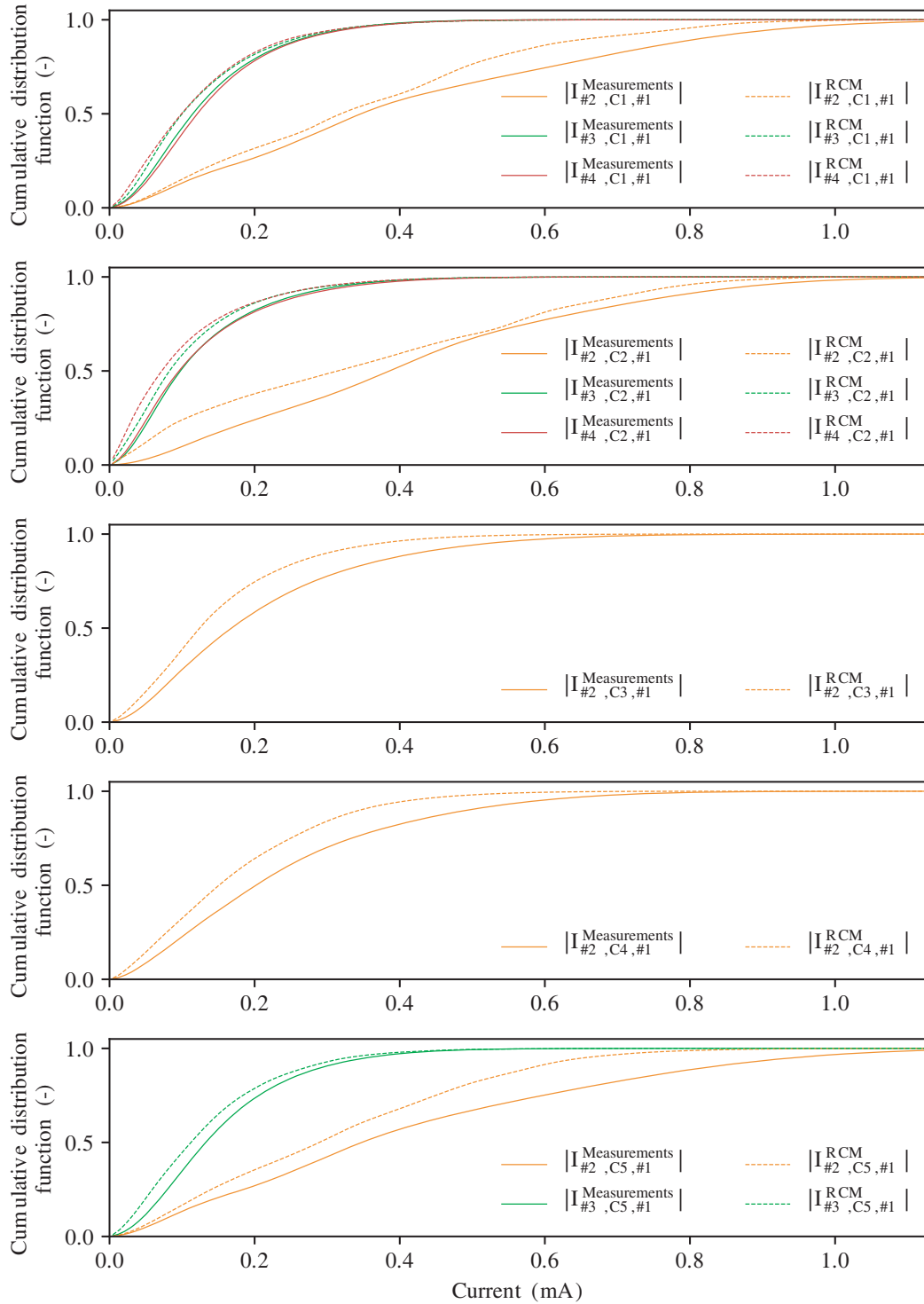


Figure 11. Cumulative distribution functions of induced currents for the five configurations. The power is injected into the port of index #1.

ones. In the line of sight case, the probability of having higher current is greater than when the source and the destination ports are not in a line of sight. In [8, 25–27], the same problem (stacking of PCB) was considered, also from an experimental point of view, and an equivalent conclusion was raised. For boards not line of sight, the RCM and the measurements data are in even better agreement.

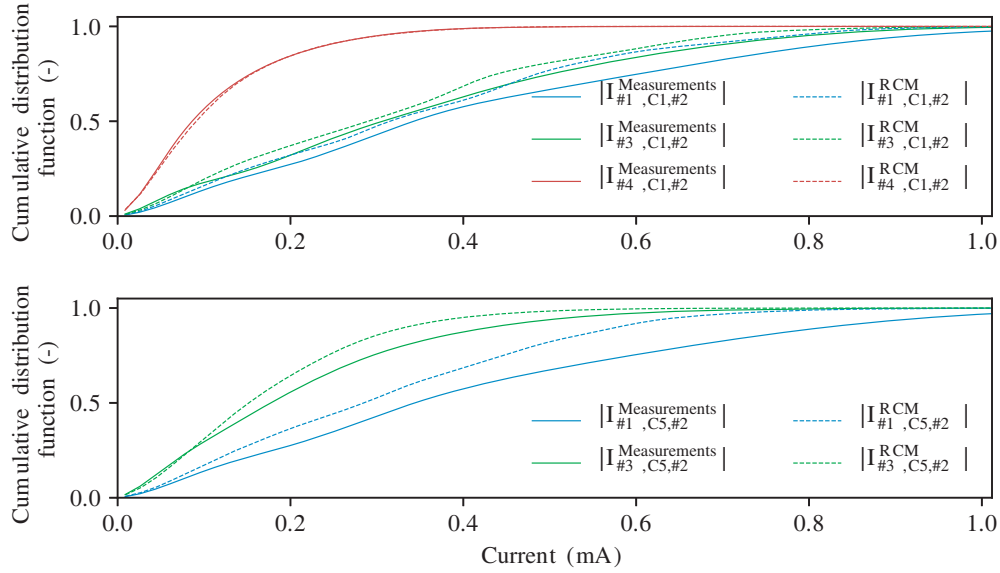


Figure 12. Cumulative distribution functions of induced currents for two configurations among five. The power is injected into the port of index #2.

Table 2. 95% percentile in μA for the five configurations with source location at port indexes #1 or #2. Fig. 10(d) indicates the four positions. Grey cells refer to line of sight configurations.

Configuration	Source port index	Position 1		Position 2		Position 3		Position 4	
		M	RCM	M	RCM	M	RCM	M	RCM
<i>C1</i>	#1 (Meander board)	Source		925	789	327	321	333	319
<i>C1</i>	#2 (Straight board)	927	787	Source		802	706	307	310
<i>C2</i>	#1 (“L right” board)	Source		883	785	321	303	336	299
<i>C2</i>	#2 (Meander board)	884	785	Source		791	733	298	301
<i>C3</i>	#1 (“L right” board)	Source		-	-	-	-	524	375
<i>C3</i>	#2 (“L left” board)	525	374	-	-	-	-	Source	
<i>C4</i>	#1 (“L right” board)	Source		-	-	595	416	-	-
<i>C4</i>	#2 (“L left” board)	594	407	-	-	Source		-	-
<i>C5</i>	#1 (Meander board)	Source		946	659	-	-	358	332
<i>C5</i>	#2 (Straight board)	948	658	Source		-	-	534	408

The higher the voltage and current magnitudes are, the higher the threat for the confidentiality of the information that an equipment processes, is. Therefore, we can analyze high percentiles of the induced currents. Table 2 lists the 95% percentiles for the five configurations, for two port source indexes (#1 and #2) and for both experimental and simulation data. When the source port is not in line of sight with the destination port, then the two percentiles (Measurements/RCM) are close.

Moreover, for all the configurations, the probability to obtain a given current amplitude is higher for the RCM than for the experimental data (i.e., $|I^{\text{Measurements}}| < |I^{\text{RCM}}|$ for all the configurations). Thus, RCM simulations tend to slightly overestimate the magnitude of the induced currents.

3.5. Effects of Absorbers on the Magnitude of Induced Currents

We will now assess the effect of adding some absorber materials inside the mock-up on the current magnitude. The boards are placed in the mock-up according to configuration *C5* (refer to Table 1).

The absorbers manufacturer indicates that the absorbers (HR-25) have a reflection coefficient less than -20 dB from 10 GHz to 60 GHz. They have been placed on the bottom of the mock-up (see Fig. 13), and the surface occupied by these is approximately of 1100 cm^2 .

The resulting CDF are depicted in Fig. 14, and again the 95% percentile are listed in Table 3. Without the absorbers, the 95% percentile is $p_{95\%, |I_{3, \text{without absorbers}}^{\text{Measurements}}|} = 372 \mu\text{A}$ for the measurement data and $p_{95\%, |I_{3, \text{without absorbers}}^{\text{RCM}}|} = 352 \mu\text{A}$ for the RCM simulations. And with the absorbers, we get $p_{95\%, |I_{3, \text{with absorbers}}^{\text{Measurements}}|} = 82 \mu\text{A}$ and $p_{95\%, |I_{3, \text{with absorbers}}^{\text{RCM}}|} = 124 \mu\text{A}$. Thus, adding a surface of 1100 cm^2 into the mock-up mitigates the magnitude of the induced current between 13.1 dB (experimental data) and 9.1 dB (RCM simulations).



Figure 13. Absorbers placed at the bottom of the mock-up. The boards are arranged according to configuration *C5*.

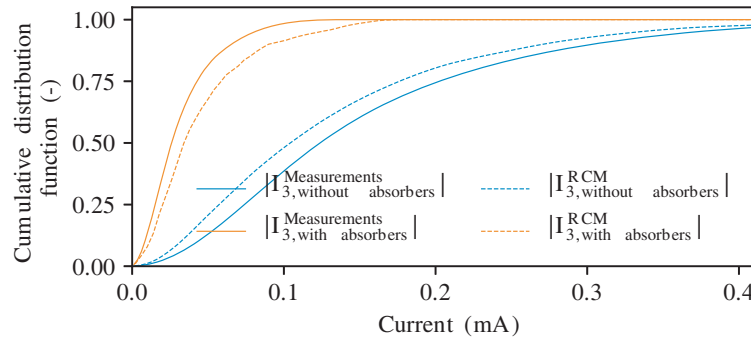


Figure 14. Induced currents with and without absorbers inside the mock-up.

Table 3. 95% percentile in μA for the configuration *C5* with and without absorbers. The source is located at port index #1.

Absorbers	with	without
	M RCM	M RCM
95% percentile	82 124	372 352

4. CONCLUSION ON ELECTROMAGNETIC ASPECTS

At first, the random coupling model has been reminded as well as its application domain (only for chaotic systems). Then, some guidelines have been given in order to efficiently implement the RCM into a compiled language. After that, a practical setup to acquire experimental data has been proposed. It is based on a computer chassis mock-up fitted with a small mode stirrer that changes the boundary conditions inside it.

Three applications of the RCM have been finally proposed. The first one is relative to the coupling between two monopoles. From experimental data, the chaoticity of the system has been assessed between 5 and 25 GHz, and we can conclude that the system can be considered as chaotic in this frequency range. The loss parameter α has been then determined for some frequencies by a fitting process. Finally, the RCM has been applied, and the probability density functions of the induced voltages, for experimental and simulated data, have been compared with good agreements.

The second application is about the stacking of several printed circuit boards with microstrip transmission lines. It addresses configurations that are more varied than previously published ones. Indeed, the ports are more complex as well as the arrangements between the ports. Induced currents have been investigated by means of cumulative distribution functions, computed from both RCM simulations and experimental data. The results have revealed two behaviors depending on whether the boards are in a line of sight or not. Comparison between the RCM simulations and experimental data has shown a good agreement for all the tested configurations.

The last study is about the effect of placing absorbers in the mock-up, and we have highlighted that adding a surface of 1100 cm² in the mock-up reduces the 95% percentile by a factor between 9.1 dB and 13.1 dB.

5. EMSEC ANALYSIS

We have illustrated that the RCM is able to quickly simulate complex reverberant environments by providing statistical quantities when the free space impedance matrix and the cavity losses are available. This study has shown that to mitigate couplings between two sensitive devices, it is necessary to interleave other non sensitive buffer boards between them. Furthermore, if the risk assessment process reveals that the magnitude of the induced current is even too high (regarding the 95% percentile for example), the insertion of absorbers inside the chassis could help to meet the requirements.

A possible application workflow, related to EMSEC is the following one. Consider the design of a new electronic equipment fitted within a chassis. Inside it, a board processing sensitive information generates parasitic signals that couple onto a given cable which should not exceed a threshold given by a risk analysis process. The first step would be to determine the free space impedance matrix $\underline{\underline{Z}}^{\text{rad}}$ between the board and the cable from a fullwave simulation software for example. Then, the quality factor Q (or the loss factor α) of the cavity should be assessed for a bandwidth depending on the spectral occupancy of the parasitic signals. Finally, the RCM may be applied to determine at what voltage/current magnitude the 95% percentile is reached.

A straightforward application is relative to encryption devices which are dedicated to encipher sensitive data. In such devices, the signal that carries the plaintext information penetrates the device from a cable, then the information is enciphered and this generated signal exits the equipment through another cable. It is thus mandatory to prevent couplings of the signal containing the plaintext (that may radiate inside the equipment chassis) to the conductor that carries the ciphered data. Indeed, if need be, the information confidentiality is not guaranteed anymore as a parasitic signal, correlated to the plaintext, will be superposed on the outgoing signal. For this situation, advantage may be taken from the RCM, as the designer of such specific equipment has the full knowledge about its constitutive elements since the making is managed from scratch. The quantity $\underline{\underline{Z}}^{\text{rad}}$ and α may thus be easily accessed.

Let's consider another situation where a server is employed to run a sensitive information system (i.e., data storage, active directory, etc.). An integrator will select commercial off-the-shelves elements (casing, hard drive, processor, ethernet controller, etc.) and will arrange these pieces of hardware together. Here, one does not control the hardware design of these elements but needs to

guarantee low couplings between two inner components like the processor and the ethernet controller. For this case, $\underline{Z}^{\text{rad}}$ and α are difficult to obtain, and it thus requires an additional modelization work.

REFERENCES

1. Backstrom, M. G. and K. G. Lovstrand, "Susceptibility of electronic systems to high-power microwaves: Summary of test experience," *IEEE Transactions on Electromagnetic Compatibility*, Vol. 46, No. 3, 396–403, 2004.
2. Berry, M. V., "Regular and irregular semiclassical wavefunctions," *Journal of Physics A: Mathematical and General*, Vol. 10, No. 12, 2083, 1977.
3. Camurati, G., S. Poeplau, M. Muench, T. Hayes, and A. Francillon, "Screaming channels: When electromagnetic side channels meet radio transceivers," *Proceedings of the 2018 ACM SIGSAC Conference on Computer and Communications Security, CCS'18*, 163–177, New York, NY, USA, 2018 (Association for Computing Machinery).
4. Cottais, E., J. L. Esteves, and C. Kasmi, "Second order soft-tempest in rf front-ends: Design and detection of polyglot modulations," *2018 International Symposium on Electromagnetic Compatibility (EMC EUROPE)*, 166–171, Aug. 2018.
5. Dyson, F. J., "A brownian-motion model for the eigenvalues of a random matrix," *Journal of Mathematical Physics*, Vol. 3, No. 6, 1191–1198, Nov. 1962.
6. Eaton, J. W., D. Bateman, S. Hauberg, and R. Wehbring, "GNU Octave version 4.2.1 manual: A high-level interactive language for numerical computations," 2017.
7. Wigner, E. P., "Random matrices in physics," *SIAM Review*, Vol. 9, No. 1, 1–23, 1967.
8. Flintoft, I. D., S. L. Parker, S. J. Bale, A. C. Marvin, J. F. Dawson, and M. P. Robinson, "Measured average absorption cross-sections of printed circuit boards from 2 to 20 GHz," *IEEE Transactions on Electromagnetic Compatibility*, Vol. 58, No. 2, 553–560, 2016.
9. Gil Gil, J., Z. B. Drikas, T. D. Andreadis, and S. M. Anlage, "Prediction of induced voltages on ports in complex, three-dimensional enclosures with apertures, using the random coupling model," *IEEE Transactions on Electromagnetic Compatibility*, Vol. 58, No. 5, 1535–1540, Oct. 2016.
10. Gradoni, G., T. M. Antonsen, S. M. Anlage, and E. Ott, "A statistical model for the excitation of cavities through apertures," *IEEE Transactions on Electromagnetic Compatibility*, Vol. 57, No. 5, 1049–1061, Oct. 2015.
11. Gradoni, G., T. M. Antonsen, S. Anlage, and E. Ott, "Theoretical analysis of apertures radiating inside wave chaotic cavities," *2012 International Symposium on Electromagnetic Compatibility (EMC EUROPE)*, 1–6, IEEE, 2012.
12. Gradoni, G., J.-H. Yeh, B. Xiao, T. M. Antonsen, S. M. Anlage, and E. Ott, "Predicting the statistics of wave transport through chaotic cavities by the random coupling model: A review and recent progress," *Wave Motion*, Vol. 51, No. 4, 606–621, 2014.
13. Guri, M., A. Kachlon, O. Hasson, G. Kedma, Y. Mirsky, and Y. Elovici, "Gsmem: Data exfiltration from air-gapped computers over GSM frequencies," *24th USENIX Security Symposium (USENIX Security 15)*, 849–864, Washington, D.C., Aug. 2015 (USENIX Association).
14. Hart, J. A., T. M. Antonsen, Jr., and E. Ott, "Effect of short ray trajectories on the scattering statistics of wave chaotic systems," *Physical review E*, Vol. 80, No. 4, 041109, 2009.
15. Hayashi, Y., N. Homma, M. Miura, T. Aoki, and H. Sone, "A threat for tablet pcs in public space: Remote visualization of screen images using em emanation," *Proceedings of the 2014 ACM SIGSAC Conference on Computer and Communications Security, CCS'14*, 954–965, New York, NY, USA, 2014.
16. Hemmady, S., T. M. Antonsen, E. Ott, and S. M. Anlage, "Statistical prediction and measurement of induced voltages on components within complicated enclosures: A wave-chaotic approach," Vol. 54, No. 4, 758–771, 2012.
17. Hemmady, S., X. Zheng, T. M. Antonsen, Jr., E. Ott, and S. M. Anlage, "Universal statistics of the scattering coefficient of chaotic microwave cavities," *Physical Review E*, Vol. 71, No. 5, 056215, 2005.

18. <http://anlage.umd.edu/RCM/>.
19. Hemmady, S. D., "A wave-chaotic approach to predicting and measuring electromagnetic field quantities in complicated enclosures," Ph.D. Thesis, University of Maryland, 2006.
20. Houchouas, V., M. Darces, N. Bourey, E. Cottais, Y. Chatelon, and M. Hélier, "Comparison between simulation and measurement of EMI inside a computer chassis mock-up," *2018 International Symposium on Electromagnetic Compatibility (EMC EUROPE)*, 551–555, Aug. 2018.
21. Kasmi, C., J. Lopes-Esteves, N. Picard, M. Renard, B. Beillard, E. Martinod, J. Andrieu, and M. Lalande, "Event logs generated by an operating system running on a cots computer during iemi exposure," *IEEE Transactions on Electromagnetic Compatibility*, Vol. 56, No. 6, 1723–1726, Dec. 2014.
22. Kuhn, M. G., "Compromising emanations of LCD TV sets," *IEEE Transactions on Electromagnetic Compatibility*, Vol. 55, No. 3, 564–570, Jun. 2013.
23. Kune, D. F., J. Backes, S. S. Clark, D. Kramer, M. Reynolds, K. Fu, Y. Kim, and W. Xu, "Ghost talk: Mitigating EMI signal injection attacks against analog sensors," *2013 IEEE Symposium on Security and Privacy*, 145–159, May 2013.
24. Mehta, M. L., *Random Matrices*, 3rd Edition, Vol. 142. Elsevier, 2004.
25. Parker, S. L., I. D. Flintoft, A. C. Marvin, J. F. Dawson, S. J. Bale, M. P. Robinson, M. Ye, C. Wan, and M. Zhang, "Changes in a printed circuit board's absorption cross section due to proximity to walls in a reverberant environment," *2016 IEEE International Symposium on Electromagnetic Compatibility (EMC)*, 818–823, 2016.
26. Parker, S. L., I. D. Flintoft, A. C. Marvin, J. F. Dawson, S. J. Bale, M. P. Robinson, M. Ye, C. Wan, and M. Zhang, "Predicting shielding effectiveness of populated enclosures using absorption cross section of PCBs," *2016 International Symposium on Electromagnetic Compatibility — EMC EUROPE*, 324–328, 2016.
27. Parker, S. L., I. D. Flintoft, A. C. Marvin, J. F. Dawson, S. J. Bale, M. P. Robinson, M. Ye, C. Wan, and M. Zhang, "Absorption cross section measurement of stacked PCBs in a reverberation chamber," *2016 Asia-Pacific International Symposium on Electromagnetic Compatibility (APEMC)*, Vol. 1, 991–993, 2016.
28. Van Eck, W., "Electromagnetic radiation from video display units: An eavesdropping risk?" *Computers & Security*, Vol. 4, No. 4, 269–286, 1985.
29. Vuagnoux, M. and S. Pasini, "Compromising electromagnetic emanations of wired and wireless keyboards," *USENIX Security Symposium*, 1–16, 2009.
30. Wand, M. P. and M. C. Jones, *Kernel Smoothing*, Chapman and Hall/CRC, 1994.
31. Yeh, J.-H., J. A. Hart, E. Bradshaw, T. M. Antonsen, E. Ott, and S. M. Anlage, "Experimental examination of the effect of short ray trajectories in two-port wave-chaotic scattering systems," *Phys. Rev. E*, Vol. 82, 041114, Oct. 2010.
32. Zheng, X., T. M. Antonsen, and E. Ott, "Statistics of impedance and scattering matrices in chaotic microwave cavities: Single channel case," *Electromagnetics*, Vol. 26, No. 1, 3–35, 2006.
33. Zheng, X., T. M. Antonsen, and E. Ott, "Statistics of impedance and scattering matrices of chaotic microwave cavities with multiple ports," *Electromagnetics*, Vol. 26, No. 1, 37–55, 2006.